D18G Transthyretin Is Monomeric, Aggregation Prone, and Not Detectable in Plasma and Cerebrospinal Fluid: A Prescription for Central Nervous System Amyloidosis?[†]

Per Hammarström,*[,‡,§] Yoshiki Sekijima,[‡] Joleen T. White,[‡] R. Luke Wiseman,[‡] Amareth Lim,[||] Catherine E. Costello,[||] Klaus Altland,[⊥] Ferenc Garzuly,[#] Herbert Budka,[▽] and Jeffery W. Kelly*[,‡]

The Skaggs Institute of Chemical Biology and Department of Chemistry, The Scripps Research Institute, BCC265, 10550 North Torrey Pines Road, La Jolla, California 92037, Mass Spectrometry Resource, Boston University School of Medicine, Boston, Massachusetts 02118, Institut für Humangenetik, Justus-Liebigs-Universität, D-35392 Giessen, Germany, Department of Neurology, Markusovszky Hospital, Szombathely, Hungary, and Institute of Neurology, University of Vienna, Vienna, Austria

Received December 9, 2002; Revised Manuscript Received March 21, 2003

ABSTRACT: Over 70 transthyretin (TTR) mutations facilitate amyloidosis in tissues other than the central nervous system (CNS). In contrast, the D18G TTR mutation in individuals of Hungarian descent leads to CNS amyloidosis. D18G forms inclusion bodies in *Escherichia coli*, unlike the other disease-associated TTR variants overexpressed to date. Denaturation and reconstitution of D18G from inclusion bodies afford a folded monomer that is destabilized by 3.1 kcal/mol relative to an engineered monomeric version of WT TTR. Since TTR tetramer dissociation is typically rate limiting for amyloid formation, the monomeric nature of D18G renders its amyloid formation rate 1000-fold faster than WT. It is perplexing that D18G does not lead to severe early onset systemic amyloidosis, given that it is the most destabilized TTR variant characterized to date, more so than variants exhibiting onset in the second decade. Instead, CNS impairment is observed in the fifth decade as the sole pathological manifestation; however, benign systemic deposition is also observed. Analysis of heterozygote D18G patient's serum and cerebrospinal fluid (CSF) detects only WT TTR, indicating that D18G is either rapidly degraded postsecretion or degraded within the cell prior to secretion, consistent with its inability to form hybrid tetramers with WT TTR. The nondetectable levels of D18G TTR in human plasma explain the absence of an early onset systemic disease. CNS disease may result owing to the sensitivity of the CNS to lower levels of D18G aggregate. Alternatively, or in addition, we speculate that a fraction of D18G made by the choroid plexus can be transiently tetramerized by the locally high thyroxine (T_4) concentration, chaperoning it out into the CSF where it undergoes dissociation and amyloidogenesis due to the low T_4 CSF concentration. Selected small molecule tetramer stabilizers can transform D18G from a monomeric aggregation-prone state to a nonamyloidogenic tetramer, which may prove to be a useful therapeutic strategy against TTR-associated CNS amyloidosis.

The amyloidoses are a large group of protein misfolding and deposition diseases, where aging is a primary risk factor. Destabilizing mutations within the amyloidogenic proteins also strongly predispose them toward amyloid formation, leading to early onset pathology. Genetic background can also influence amyloidosis, especially genes controlling the concentration of macromolecular and small molecule ligands that bind to and stabilize the amyloidogenic protein against misfolding. The amyloidogenic protein transthyretin (TTR)[1] is synthesized in the liver, the choroid plexus, and the retina of the eye. TTR is a β-sheet-rich homotetramer that carries the holoretinol binding protein (holoRBP) and thyroxine (T_4) in the plasma and CSF. WT TTR amyloidosis requires rate-limiting tetramer dissociation and partial monomer denaturation, producing an intermediate that misassembles into amyloid and other structures. In the over 70 mutations that cause familial amyloid polyneuropathy (FAP), the patients initially present with peripheral neuropathy and autonomic dysfunction that subsequently progress toward systemic amyloidosis. Elderly people with senile systemic amyloidosis

[†] Support from the National Institutes of Health (DK 46335 to J.W.K. and P41-RR10888 to C.E.C.), The Skaggs Institute of Chemical Biology (to J.W.K.), and The Lita Annenberg Hazen Foundation (to J.W.K.) and a postdoctoral fellowship to P.H. from the Wenner-Gren Foundations is appreciated.

* Corresponding authors.
[‡] The Scripps Research Institute.
[§] Present address: IFM Department of Chemistry, Linköping University, SE-581 83 Linköping, Sweden.
[||] Boston University School of Medicine.
[⊥] Justus-Liebigs-Universität.
[#] Markusovszky Hospital.
[▽] University of Vienna.

[1] Abbreviations: TTR, transthyretin; D18G, TTR with an aspartate to glycine substitution at position 18; FT_2-TTR, TTR with a tandem copy of the FLAG sequence DYKDDDDKDYKDDDDK attached to its N-terminus; M-TTR, a F87M/L110M TTR variant that is monomeric under physiological conditions at micromolar concentrations; T_4, L-thyroxine; holoRBP, retinol binding protein with retinol (vitamin A) bound; CSF, cerebrospinal fluid; CNS, central nervous system; LT, liver transplantation.

10.1021/bi027319b CCC: $25.00
Published on Web 05/16/2003

(SSA) often have cardiac amyloid deposits composed of the WT protein (*1*; in 10−25% of people over age 80), whereas the V122I mutation can lead to familial amyloid cardiomyopathy (FAC) in ≈4% of African Americans (*2*) around the seventh decade. FAP and FAC are autosomal dominant disorders, implying that coexpression of variant and WT TTR in heterozygotes leading to hybrid TTR tetramer formation is sufficient for pathology with variable penetrance. There is no evidence that these are loss of function diseases; instead, they appear to operate by a gain of toxic function mechanism associated with the predominant aggregation of destabilized variants of TTR.

It is rare to find TTR amyloidosis patients with CNS involvement, unlike the situation in Alzheimer's disease. However, D18G TTR heterozygotes of Hungarian descent present with primary CNS involvement in the fifth decade. They have extensive amyloid deposition in the leptomeningeal vessels and in the subarachnoid membrane, with asymptomatic non-CNS deposition in the kidney, heart, and skin (*3*−*5*). Herein, we describe the biophysical properties of D18G TTR, beginning with the observation that it is an unstable monomeric protein that is aggregation prone under physiological conditions. Its low stability may protect D18G carriers from early onset non-CNS disease by impairing secretion efficiency and/or enhancing catabolic clearance. Analysis of patient's serum and cerebrospinal fluid (CSF) was unable to detect the D18G protein, supporting this hypothesis. Unlike other sequences studied to date, D18G TTR is very inefficient at making hybrid tetramers with WT TTR subunits, a feature that likely contributes to our inability to detect D18G in serum. T_4 binding facilitates tetramerization of D18G at the high concentrations that may be found in the choroid plexus but not at the concentrations found in the CSF. Ironically, it may be the small amount of T_4-tetramerized D18G TTR that ends up misfolding in the CNS.

MATERIALS AND METHODS

Protein Expression and Purification. Expression and purification were performed as described previously (*6*). Recombinant expression of WT, L55P, V30M, V122I, and T119M TTR homotetramers in *Escherichia coli* at 37 °C produces soluble native tetrameric protein. However, recombinant expression of D18G, V30M M-TTR and L55P M-TTR forms inclusion bodies upon expression in *E. coli* at 37 °C. HoloRBP was prepared as described previously (*7*).

Purification of D18G, V30M M-TTR and L55P M-TTR TTR from Inclusion Bodies. Transformed Epicurian gold *E. coli* (Stratagene) (4 × 1 L) were grown at 37 °C for 4−5 h until the OD^{660} reached ≈1. Protein expression was induced by 1 mM IPTG, and expression proceeded for 12 h at 37 °C. The cells were lysed by sonication (4 × 3 min) on ice in the presence of 1 mM phenylmethanesulfonyl fluoride (PMSF) and 5 mM EDTA. The lysate was centrifuged at 18000 rpm for 30 min. The pellet was resuspended in 40 mL of "inclusion body buffer" (IB) (1.5 M NaCl, 50 mM EDTA, 1% Triton X, pH 7.4) and centrifuged again. The IB wash was repeated once. Thereafter, the pellet was washed in TBS, and the protein was unfolded by dissolving the washed pellet in 40 mL of 8 M GdmCl (50 mM phosphate, pH 7.4, 100 mM DTT). The unfolding reaction proceeded for 48 h at 4 °C with stirring. Unfolded TTR (20 mL) was refolded by dilution at 4 °C into 1600 mL of 10% glycerol, 50 mM phosphate, 100 mM KCl, 1 mM PMSF, and 5 mM EDTA (<0.1 M GdmCl and <0.05−0.15 mg/mL protein). After a 30 min incubation period, the refolded protein was concentrated and dialyzed against 50 mM phosphate, 100 mM KCl, 1 mM DTT, 5 mM EDTA, and 1 mM PMSF (pH 7.2). The protein was filtered (0.2 μm) and purified using a Superdex 75 gel filtration column. The masses of the proteins were confirmed by ESI-MS, and the purity was established by SDS−PAGE. The monomers were stored at 4 °C (0.1−0.5 mg/mL). The total yield of pure monomeric protein was 3−5 mg/L of culture media.

Mass Spectrometry. LC-ESI-MS analysis was performed using a Hewlett-Packard 1100-MSD mass spectrometer, running a linear gradient of acetonitrile/water (0−100% MeCN) acidified with TFA (0.05%) or formic acid (0.1%). The masses of the recombinant proteins in this study were as follows: WT-TTR, 13892 ± 1 Da; D18G, 13834 ± 1 Da; L55P M-TTR,: 13877 ± 1 Da; V30M M-TTR, 13925 ± 1 Da; and FT_2-WT TTR, 15882 ± 2 Da. (All our recombinant TTR variants contain an extra Met at the N-terminus.)

TTR was immunoprecipitated from the serum of a normal control individual and of the patient diagnosed with D18G TTR amyloidosis. The immunoprecipitated samples were HPLC purified and mass analyzed using a Micromass Quattro II triple quadrupole mass spectrometer as described previously (*8*).

Analysis of the Sedimentation Velocity Profiles of D18G TTR with Ligands. Freshly prepared solutions of D18G TTR (28.8 μM monomeric concentration) were incubated with holoRBP (7.2 μM) and/or T_4 or 2-[(3,5-dichlorophenyl)-amino]benzoic acid (28.8 μM) for 2 h at room temperature in 10 mM sodium phosphate, 100 mM KCl, and 1 mM EDTA (pH 7.6). Controls of D18G TTR and holoRBP alone were also prepared. Sedimentation velocity profiles were obtained on a temperature-controlled Beckman XL-I analytical ultracentrifuge (Beckman Coulter, Fullerton, CA) equipped with an An50Ti rotor and a photoelectric scanner. Data at 330 nm [for samples containing holoRBP as described previously (*7*)] and 280 nm (for samples without RBP) were collected at rotor speeds of 3000 rpm initially and 50000 rpm in a continuous mode at 20 °C, with a step size of 0.003 cm.

Evaluation of the data was performed using the program DCDT+, in which multiple data sets (concentration vs radial position) taken at various times during the experiment were used to calculate the time derivative (*9*). This was thereafter used to determine the sedimentation coefficient distribution function $g(s^*)$. By fitting Gaussian functions to the $g(s^*)$ distribution, the sedimentation and diffusion coefficients, and therefore molecular masses, were determined. The data were fitted to one, two, or three noninteracting species.

Recombinant Coexpression. Coexpression of D18G and FT_2-WT TTR was performed as described previously (*10*). Purification of the soluble fraction was performed as described previously (*11*), and purification of insoluble material (inclusion bodies) was performed as described above. Protein identification was accomplished by ESI-MS.

Small Molecule Binding Induced TTR Tetramerization Analyzed by Gluteraldehyde Cross-Linking and SDS−PAGE.

2-[(3,5-Dichlorophenyl)amino]benzoic acid and 2-[(3,5-dichlorophenyl)amino]benzeneacetic acid were synthesized as described (*12*). T_4, resveratrol, diclofenac, and 3,3′,5,5′-tetrachlorobiphenyl-4,4′-diol were obtained from Sigma. 4-[[2-(Trifluoromethyl)phenoxyimino]methyl]benzoic acid was synthesized by H. M. Petrassi (unpublished). D18G samples (0.20 mg/mL, 14.4 μM monomer) were incubated for 24 h in the presence of small molecule inhibitors (28.8 μM). Glutaraldehyde cross-linking of the protein was performed by taking out 50 μL samples to which was added 5 μL of glutaraldehyde (25%). The cross-linking reaction was allowed to proceed for 3 min before quenching by addition of 5 μL of $NaBH_4$ (7% in 0.1 M NaOH). The samples were mixed with 20 μL of SDS reducing gel loading cocktail (final SDS concentration = 2.5%) and boiled for 5 min before the electrophoresis gel was loaded. The cross-linked protein was visualized by Coomassie R-250 staining.

Subunit Exchange. Monomeric D18G (4 μM) was incubated with FT_2-WT TTR (1 μM tetramer) at 4 °C. The extent of hybrid tetramer formation was evaluated by analytical anion-exchange chromatography as described previously (*10*, *11*).

CD, Fluorescence, and Stability Measurements. Far-UV CD spectra of 0.10 mg/mL TTR samples in a 2 mm cuvette were obtained using an AVIV SF-202 circular dichroism spectrometer. Fluorescence spectra were collected on an AVIV ATF-105 spectrofluorometer, following excitation at 295 nm. Stopped-flow fluorescence (25 °C) was recorded at 335 and 355 nm following excitation at 290 nm. Urea stability measurements (25 °C) were perfomed on TTR samples (0.02 mg/mL) using the tryptophan fluorescence intensity ratio at 335 and 355 nm as the structural probe as described previously (*13*−*16*). For the refolding data, D18G was denatured for 48 h in 6.0 M urea prior to dilution to the final urea concentrations. The data for unfolding of M-TTR (*16*) and monomeric D18G were fitted to a two-state model: M^F (folded monomers) $\leftrightarrow$ M^U(unfolded monomers). The fraction of unfolding (F_U) was calculated by the formula $F_U = (I^{355/335}_N - I^{355/335})/(I^{355/335}_N - I^{355/335}_U)$, where $I^{355/335}_N$ is the dependence of the pretransition baseline fluorescence ratio on urea concentration [355 (unfolded maximum)/335 nm (folded maximum)]. $I^{355/335}$ is the fluorescence ratio for measured data points in the transition region, and $I^{355/335}_U$ is the posttransition baseline dependence on urea concentration. The Gibbs free energy of the reaction was calculated by the formula $\Delta G_{NU} = -RT \ln[F_U/(1 - F_U)]$ and was assumed to be linearly dependent on the urea concentration according to $\Delta G_{NU} = \Delta G_{NU}^{H_2O} - m$[urea].

Fibril Formation Assays. Fibril formation kinetics were evaluated by mixing equal volumes of D18G TTR in 10 mM phosphate buffer (pH 7.0) containing 100 mM KCl, 1 mM DTT, and 1 mM EDTA (in the presence or absence of T_4, preincubated for 2 h) with 100 mM acetate buffer (pH 4.8) containing 100 mM KCl and 1 mM EDTA (to yield a final pH of 5.0 and a TTR concentration of 0.2 mg/mL in a UV cuvette). The OD at 330 and 400 nm was monitored with stirring at 37 °C. After the turbidity assay, the samples were centrifuged, and the pellet was resuspended in 50 mM phosphate buffer (pH 7.0). Thioflavin T (10 μM, ThT) was added, and the fluorescence was recorded (450−550 nm following 440 nm excitation).

Table 1: TTR Sequences and States after Recombinant Overexpression in *E. coli* (37 °C)[a]

TTR sequence	state[b]	TTR sequence	state[b]
WT	sol	M-TTR	sol
D18G	ib	V30M M-TTR	ib
V30M	sol	L55P M-TTR	ib
L55P	sol	V122I M-TTR	sol
T119M	sol	T119M M-TTR	sol
V122I	sol		

[a] Expression of TTR variants in Epicurian gold (Stratagene) BL21/DE3 was performed as described in Materials and Methods. Lysis was accomplished by sonication, and solubility was established following centrifugation at 18000 rpm for 30 min. [b] Inclusion bodies = ib and soluble = sol.

D18G, WT TTR, V30M M-TTR, and L55P M-TTR amyloid formation as a function of pH was evaluated by incubating the protein at various pHs by mixing equal volumes of TTR in 10 mM phosphate buffer (pH 7.0) containing 100 mM KCl, 1 mM DTT, and 1 mM EDTA with 100 mM citrate buffer (in the pH range 3.2−3.8), 100 mM acetate buffer (in the pH range 4.0−5.6), or 100 mM phosphate buffer (in the pH range 6.2−7), all containing 100 mM KCl and 1 mM EDTA. The OD at 330 and 400 nm was measured following incubation (72 h, 37 °C).

RESULTS

Inclusion Body Formation. Recombinant expression of WT, L55P, V30M, V122I, and T119M TTR homotetramers in *E. coli* at 37 °C each provides 30−50 mg/L of culture media of soluble purified native tetrameric protein (*14*). In contrast, expression of D18G TTR results in inclusion body formation. Purification of D18G from inclusion bodies was accomplished as described in the Materials and Methods section. Purity and identity were assessed by SDS−PAGE and ESI-MS (MW = 13834 ± 1), respectively. Interestingly, expression of engineered monomeric variants of L55P TTR (L55P/F87M/L110M = L55P M-TTR) and V30M TTR (V30M/F87M/L110M = V30M M-TTR) also formed inclusion bodies in contrast to the wild-type TTR monomer (F87M/L110M = M-TTR) and monomers with more stable tertiary structures (Table 1).

D18G Is Predominantly Monomeric. Gel filtration analysis of D18G TTR shows that soluble aggregates and monomeric protein coexist after storage. Analytical ultracentrifugation data on freshly purified protein at a concentration of 28.8 μM reveal that D18G TTR is >94% monomeric, exhibiting a sedimentation coefficient ($s_{20,w}$) = 1.7−1.9 and a fitted molecular mass of 13.96 ± 0.28 kDa (Table 2, Figure 1A). The soluble aggregates formed after storage sediment immediately upon initiation of the analytical ultracentrifugation run at 3000 rpm, implying that their molecular mass exceeds 500 kDa. Dialysis of these high MW soluble aggregates against 10 mM HCl (pH 2) in distilled H_2O (no salt) at 4 °C followed by ESI-MS demonstrates that the aggregates are composed of pure unmodified D18G TTR (MW = 13834).

Structural Characterization. The far-UV CD spectrum of freshly purified D18G TTR (7.2 μM) exhibits a minimum at 214 nm similar to WT TTR, consistent with its β-sheet-rich structure (Figure 2A). The intensity of the minimum is lower, possibly indicating a less structured monomer. However, the fluorescence spectra of WT (maximum at 338

Table 2: D18G Quaternary Structural Analysis by Sedimentation Velocity Studies[a]

	% monomer (13.5 kDa)[b]	% tetramer (55 kDa)[c]	% oligomer (110 kDa)[d]
D18G (28.8 μM)[f]	94 ± 1	6 ± 1[e]	
D18G (28.8 μM) + T_4 (28.8 μM)[g]	43 ± 2	43 ± 1	14 ± 1
D18G (28.8 μM) + 2-[(3,5-dichlorophenyl)-amino]benzoic acid (28.8 μM)[g]	48 ± 1	52 ± 1	

[a] Sedimentation velocity experiments (monitored at 280 nm) to evaluate binding of D18G TTR (28.8 μM) to small molecule ligands (28.8 μM). The time-dependent concentration versus radial distance data were fitted to a three-species model of TTR monomer, tetramer, and oligomer. The relative concentrations and sedimentation coefficients (SC, in Svedberg units) were obtained from Gaussian curves fitted to the $g(s^*)$ sedimentation coefficient distribution using the molecular masses of the three species. [b] SC = 1.77 ± 0.28. [c] SC = 3.83 ± 0.25. [d] SC = 5.52 ± 0.05. [e] This species is possibly a non-native oligomer. [f] Sample not preincubated at 20 °C prior to measurement to minimize aggregation. [g] Samples preincubated with ligands for 2 h at 20 °C.

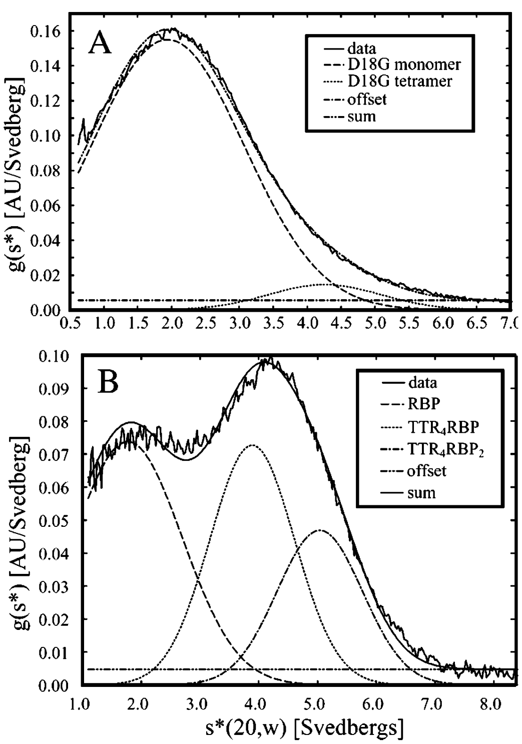

FIGURE 1: (A) Sedimentation velocity data for D18G TTR (28.8 μM) monitored at 280 nm. The data were fitted to a two-species model of TTR monomer and tetramer. (B) Velocity data for D18G TTR (28.8 μM) preincubated with L-thyroxine (T_4) (28.8 μM) and holoRBP (7.2 μM), monitored at 330 nm (retinol absorbance). The data were fitted to a three-species model of RBP monomer, TTR tetramer/RBP, and TTR tetramer/RBP_2.

nm) and D18G TTR (maximum at 339 nm) are virtually identical (Figure 2B, 7.2 μM), implying similar environments and, by extension, folds in the vicinity of W41. While TTR has two tryptophan residues (W41 and W79), the signal in the native protein originates from W41 owing to internal quenching of W79 (*17*). The urea denaturation curve of D18G TTR monitored by Trp fluorescence is depicted in Figure 2C. The fully reversible unfolding transition is cooperative with a C_m at 1.85 ± 0.05 M urea. Calculating the free energy of D18G unfolding [$\Delta G_{NU}^{H_2O}$ = 2.4 ± 0.2

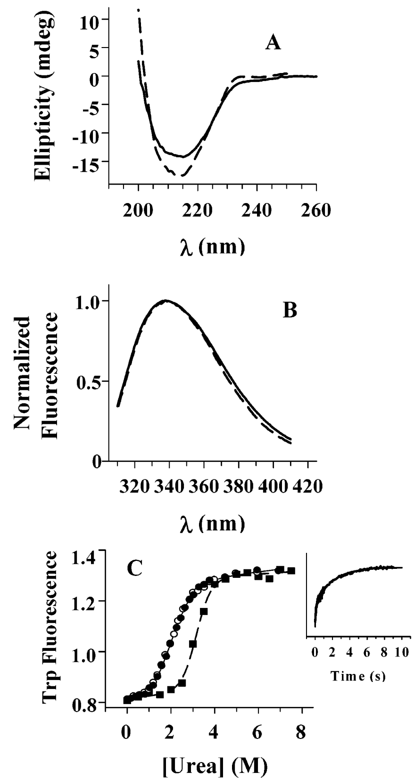

FIGURE 2: (A) Structural characterization by far-UV CD and (B) Trp fluorescence spectra of D18G (solid line) and WT TTR (dashed line). (C) Urea stability measured by Trp fluorescence. D18G unfolding (filled circles) and D18G refolding (open circles) curves are superimposable. The previously published unfolding curve for M-TTR (*16*) is shown for comparison (filled squares, dashed line). The inset in (C) shows the unfolding kinetics of D18G in 3.0 M urea.

kcal mol^{-1} (m = 1.3 ± 0.1 kcal mol^{-1} M^{-1})] compared to that of monomeric M-TTR previously reported (*16*) [C_m at 3.2 M urea and a $\Delta G_{NU}^{H_2O}$ = 5.5 ± 0.8 kcal mol^{-1} (m = 1.7 ± 0.2 kcal mol^{-1} M^{-1})] reveals that its tertiary structure is 3.1 kcal mol^{-1} less stable in water (25 °C).

Rapid Denaturation Kinetics of D18G. Importantly, D18G is unable to tetramerize at physiological concentrations (14.4 μM monomeric TTR), resulting in dramatic kinetic destabilization of the mutant relative to tetrameric WT TTR under denaturing conditions (*14*). The WT protein exhibits an apparent unfolding half-time of 20 h in 6.0 M urea (25 °C), owing to rate-limiting tetramer dissociation (*14*). In comparison, the destabilized L55P tetramer dissociates 10-fold faster but still requires hours (*14*). A stopped-flow trace for the unfolding of D18G TTR (3.0 M urea), shown in the inset of Figure 2C, reveals that it is at least 500000-fold faster than WT (6.0 M urea). The process is biphasic (for unknown reasons); nevertheless, an average of the amplitudes and rate constants of both phases yields an average rate constant of unfolding of 4.9 s^{-1} (half-time of 140 ms) (25 °C). Previous studies demonstrate that fast unfolding kinetics of TTR translates to rapid fibril formation rates. Monomeric M-TTR behaves similarly to D18G TTR (*14*) because tetramer dissociation is no longer rate limiting.

D18G Rapidly Aggregates at Neutral pH. Figure 3A summarizes the pH-dependent aggregation properties of monomeric D18G relative to WT TTR. The D18G TTR variant exhibits a very broad pH aggregation profile which is shifted to significantly higher pH than that characterizing

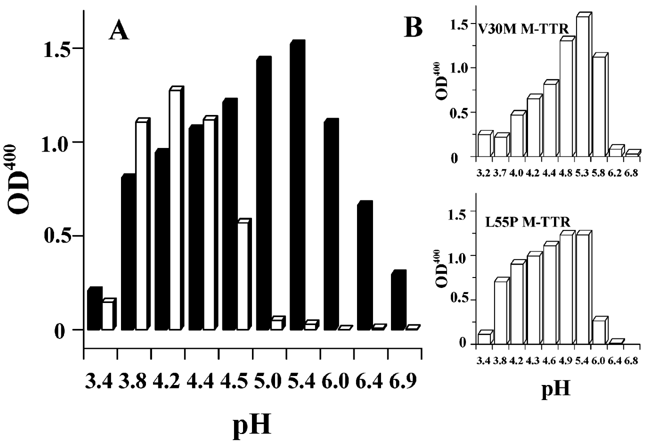

FIGURE 3: TTR aggregation as a function of pH. (A) pH profiles of D18G (black columns) and WT TTR (white columns) demonstrate the higher pH amyloidogenicity of D18G after 72 h. (B) pH profiles of V30M M-TTR (top panel) and L55P M-TTR (bottom panel) aggregation.

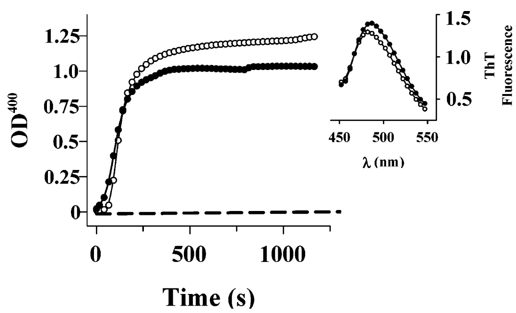

FIGURE 4: D18G (0.20 mg/mL) fibril formation kinetics (pH 5.0, 37 °C) with (filled circles) and without (open circles) T_4 (28.8 μM). For comparison the dashed line shows the WT TTR (0.20 mg/mL) fibril formation time course (pH 4.4, 37 °C). The inset shows the ThT fluorescence for the D18G samples after 2 h of incubation.

WT TTR. Whereas WT TTR requires 72 h to exhibit a maximum in amyloid fibril formation (pH 4.4, 37 °C) (*14*), the D18G variant exhibits maximal deposition in 3 min (pH 5.0, 37 °C, Figure 4), a 1000-fold rate acceleration. D18G aggregates 4-fold faster than M-TTR (pH 4.4, 37 °C) (*16*), probably owing to further tertiary structural destabilization and/or faster assembly of the partially folded D18G intermediate. The pH profiles of V30M M-TTR and L55P M-TTR resemble D18G (Figure 3B); however, they show less aggregation above pH 6.

D18G TTR Is Not Detected in Patient's Serum and CSF. We analyzed the TTR concentration in the serum and CSF from a heterozygous D18G patient. Whereas the total protein concentration in serum was normal (77 mg/mL), the TTR concentration was remarkably low (0.06 mg/mL) in comparison to WT TTR homozygotes (0.2−0.4 mg/mL). We employed isoelectric focusing and mass spectrometry to quantify the D18G:WT TTR ratio. Isoelectric focusing is sensitive enough to detect TTR variants including those with substitutions not involving changes in the overall charge (*18*). However, no D18G was found using this approach. Similarly, only WT TTR could be detected in the serum utilizing mass spectrometry (Supporting Information, Figure 1). This is unusual because mass spectrometry usually detects the mutant protein in patients' sera (e.g., V30M, V30L, F33L, D38A, S50R, A97G, and A97S) (*19*). Even the L55P amyloidogenic TTR mutation leading to the earliest onset disease is detectable in serum (*20*). The CSF exhibited a very high total protein concentration (8.8 mg/mL; normal <0.45 mg/mL) with a TTR concentration of 0.04 mg/mL (normal 0.01 mg/mL). However, the D18G TTR variant could not be detected in the CSF either. The elevated level of TTR and total protein in the CSF is most likely due to the impairment of the blood−brain barrier as a consequence of the severe amyloid deposition in the leptomeningeal vessels.

Can D18G and WT TTR Subunits Form Hybrid Tetramers? Simulating Heterozygote Expression. The D18G carriers are heterozygotes; hence both WT TTR and D18G TTR should be expressed in similar amounts in the liver and the choroid plexus. If D18G behaves like other disease-associated variants studied to date, coexpression results in hybrid tetramer formation. However, as outlined above only WT TTR is detected in CSF and plasma. To simulate this situation, D18G and FT_2-WT TTR were coexpressed in *E. coli* using a method described previously (*10*). Analysis of the composition of soluble purified TTR and the inclusion bodies in *E. coli* using ESI-MS revealed that the soluble fraction contained exclusively FT_2-WT protein—no D18G TTR (Supporting Information, Figure 2). The TTR in the insoluble fraction was composed of >80% D18G TTR (<20% FT_2-WT). These results imply that mixed TTR tetramers cannot protect the D18G variant from aggregation and/or suggest that the formation of soluble hybrid tetramers composed of WT and D18G in vivo is a very inefficient process. To further address whether D18G TTR is competent to form hybrid tetramers with WT TTR, we performed subunit exchange experiments at a protein concentration (4 μM monomer) and temperature (4 °C) previously established to suppress aggregation and enhance subunit exchange (*11*). The formation of mixed tetramers can easily be detected and quantified by analytical anion-exchange chromatography because FT_2-WT TTR has an N-terminal anionic tail (*10*, *11*). Figure 5A demonstrates that minimal D18G/WT hybrid tetramer formation occurs on a time scale where the V30M/WT and L55P/WT exchange reactions are complete. The latter two examples yield a statistical distribution (1:4:6:4:1) of the five hybrid tetramers (*11*). The distribution resulting from mixing D18G/WT TTR is highly biased toward tetramers containing FT_2-WT subunits with the homotetrameric FT_2-WT predominating even after 42.5 h (Figure 5A). No D18G homotetramer is detected (peak 1) (Figure 5A). The hybrid tetramer distribution after 42.5 h reveals only 0.6% of $(D18G)_3(WT)_1$ (peak 2), 5% of $(D18G)_2(WT)_2$ (peak 3), and 25% of $(D18G)_1(WT)_3$ (peak 4) (Figure 5B), suggesting that D18G-containing hybrid tetramers are very unstable.

Can T_4 or HoloRBP Tetramerize D18G TTR? Sedimentation velocity studies were used to evaluate the distribution of D18G TTR quaternary structures (28.8 μM) as a function of added tetramer binding ligands. The fraction D18G tetramer increases to as much as 50% when incubated with small molecules [T_4 or 2-[(3,5-dichlorophenyl)amino]benzoic acid] (Table 2). The ligand 2-[(3,5-dichlorophenyl)amino]-benzoic acid prevents the formation of higher order D18G aggregates more efficiently than T_4. HoloRBP, a TTR ligand previously shown to transform monomeric M-TTR into a tetramer (*16*), is only able to tetramerize 20% of D18G (Table 3). In the presence of bound small molecules, holoRBP is able to bind D18G to a greater extent (Table 3)

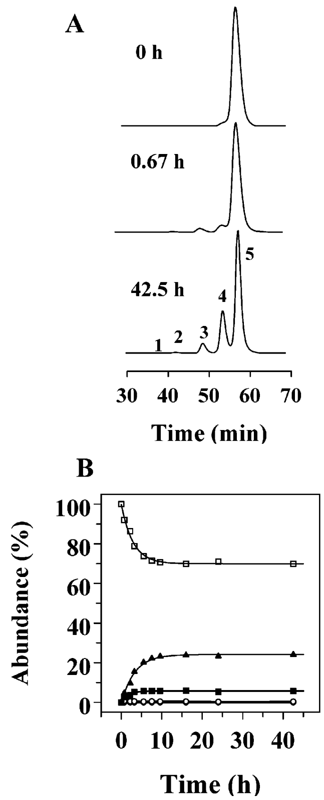

FIGURE 5: Subunit exchange between D18G monomers and FT_2-WT TTR homotetramers as a function of time (4 °C). (A) Chromatographic traces from analytical anion exchange after 0, 0.67, and 42.5 h of exchange. The numbers on the lower trace indicate the elution position of the five different tetramers. (B) Abundance of each hybrid tetramer as a function of time. Peak 2 composed of $(D18G)_3(WT)_1$ is represented by open circles, peak 3 composed of $(D18G)_2(WT)_2$ is represented by filled squares, peak 4 composed of $(D18G)_1(WT)_3$ is represented by filled triangles, and peak 5 composed of $(WT)_4$ is represented by open squares.

(Figure 1B). The small molecule 2-[(3,5-dichlorophenyl)-amino]benzoic acid is superior to T_4 in terms of enhancing RBP binding, consistent with its tetramerization efficacy.

D18G Tetramer Formation Induced by Small Molecule Binding, Inhibiting Aggregation. Under denaturing conditions (pH 5.0, 37 °C) D18G TTR readily aggregates, forming both amyloid and amorphous aggregates. D18G TTR preincubated with T_4 (29 μM) is not significantly protected against rapid aggregation as ascertained by turbidity and ThT fluorescence (Figure 4). Seven small molecule TTR tetramer binders including T_4 (28.8 μM) were added to monomeric D18G TTR (14.4 μM), and their ability to induce tetramer formation at neutral pH was evaluated by SDS−PAGE employing chemical cross-linking. In the absence of inhibitor, the protein forms soluble aggregates (>190 kDa) (20 °C, 24 h) and cannot enter the gel. However, most small molecule inhibitors are effective at tetramerizing D18G TTR, thereby preventing aggregation at 20 °C (Figure 6). T_4 can drive 50% of the D18G TTR to tetramer, the remainder being aggregates. At a higher concentration of T_4 (288 μM) it is still the least effective inhibitor in the group (Figure 6). At 37 °C almost every small molecule inhibitor is rather ineffective owing to increased efficiency of aggregation, the exception being the 3,3′,5,5′-tetrachlorobiphenyl-4,4′-diol (lane 4), which drives D18G almost completely to tetramer and protects D18G against aggregation including amyloid fibril

Table 3: HoloRBP/D18G Quaternary Structural Analysis by Sedimentation Velocity Studies[a]

	% holoRBP (21 kDa)[b]	% TTR tetramer/holoRBP (76 kDa)[c]	% TTR tetramer/$holoRBP_2$ (97 kDa)[d]
holoRBP (7.2 μM)	100 ± 1		
D18G (28.8 μM) + holoRBP (7.2 μM)[e]	80 ± 1	20 ± 1	
D18G (28.8 μM) + T_4 (28.8 μM) + holoRBP (7.2 μM)[e]	44 ± 1	34 ± 1	22 ± 1
D18G (28.8 μM) + 2-[(3,5-dichlorophenyl)-amino]benzoic acid (28.8 μM) + holoRBP (7.2 μM)[e]	30 ± 1	45 ± 1	25 ± 1

[a] Sedimentation velocity experiments (monitored at 330 nm) to evaluate binding of D18G TTR (28.8 μM) to RBP (7.2 μM) in the presence or absence of small molecule ligands (28.8 μM). The time-dependent concentration versus radial distance data were fitted to a three-species model of RBP monomer, TTR/holoRBP, and TTR/$holoRBP_2$. The relative concentrations and sedimentation coefficients (SC, in Svedberg units) were obtained from Gaussian curves fitted to the $g(s^*)$ sedimentation coefficient distribution using the molecular masses of the three species. [b] SC = 1.85 ± 0.19. [c] SC = 3.74 ± 0.18. [d] SC = 5.26 ± 0.23. [e] Samples preincubated with ligands for 2 h at 20 °C.

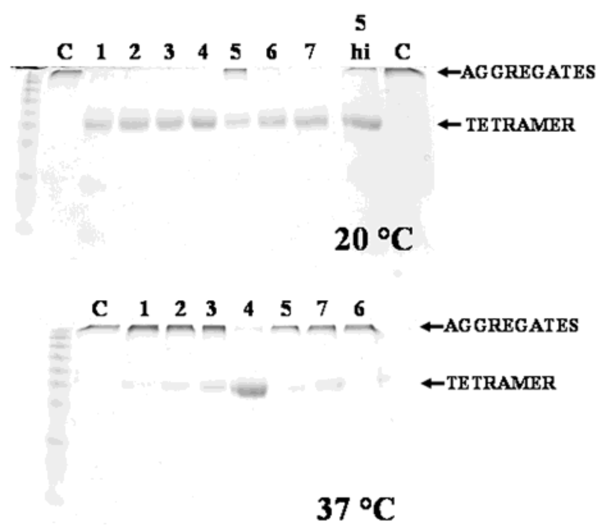

FIGURE 6: SDS−PAGE gel analysis of cross-linked D18G after incubation of D18G (14.4 μM monomer) at 20 °C (top gel) and 37 °C (bottom gel) in the absence (C = control) and in the presence of 28.8 μM **1** (diclofenac), **2** (resveratrol), **3** [2-[(3,5-dichlorophenyl)amino]benzeneacetic acid], **4** (3,3′,5,5′-tetrachlorobiphenyl-4,4′-diol), **5** [L-thyroxine (T_4)], **6** [4-[[2-(trifluoromethyl)phenoxyimino]methyl]benzoic acid], and **7** [2-[(3,5-dichlorophenyl)amino]-benzoic acid] or 288 μM **5** hi [L-thyroxine (T_4)].

formation. This molecule binds WT TTR with high affinity; K_{d1} and $K_{d2} \approx 3$ nM by isothermal titration calorimetry (H. Purkey et al., unpublished results).

DISCUSSION

D18G is the most unstable disease-associated TTR variant reported to date, consistent with its inclusion body formation in *E. coli*. The tetramer is so destabilized that it does not form to an appreciable extent at physiological protein concentration and pH. The protein is >94% monomeric

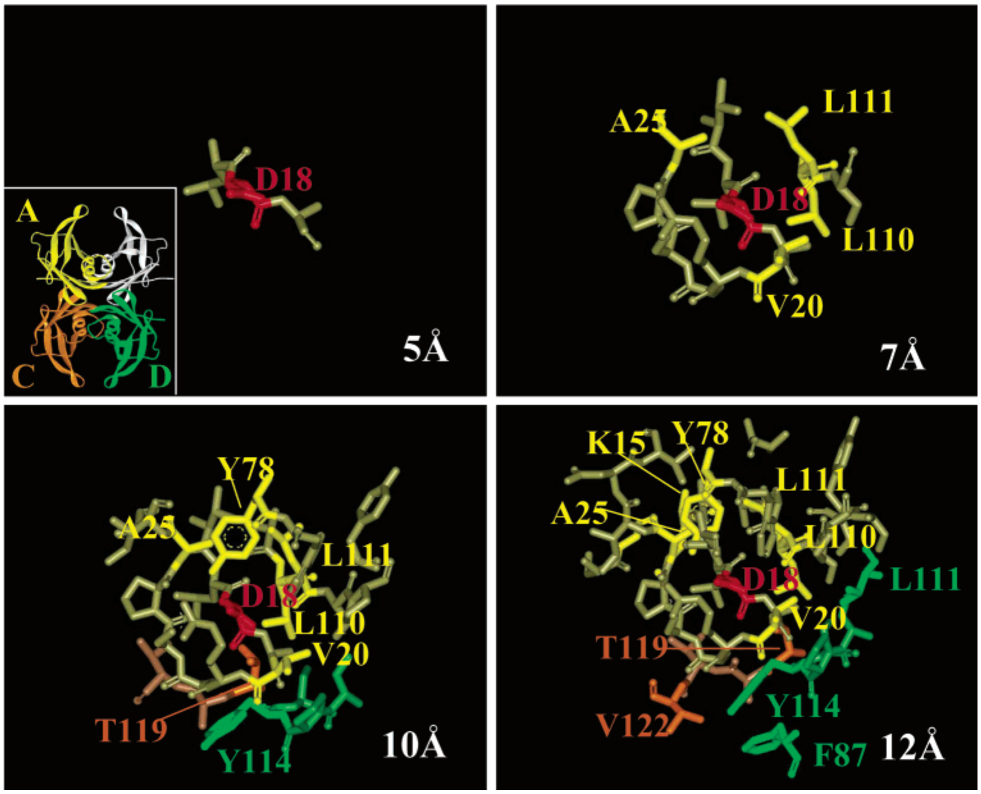

FIGURE 7: Residues within a radius of 5, 7, 10, and 12 Å from the C_α of residue D18 (red). Residues known to influence TTR tetramer stability and/or mutation sites with a relevant clinical phenotype are highlighted. The colors indicate which subunit the residues are located within following the scheme shown in the inset. Yellow indicates that the residue is within the same subunit as the reference D18 amino acid (cis) (labeled A in inset). Orange residues are located in the neighboring subunit of the face to face dimer interface (labeled C in inset). Green residues are located in subunit D (see inset).

according to sedimentation velocity analysis, and while it appears to adopt a normal fold, its tertiary structure is destabilized relative to monomeric M-TTR by 3.1 kcal/mol. The rate-limiting step of WT TTR unfolding and fibril formation is tetramer dissociation, but since D18G is a monomer, it unfolds 500000-fold faster and aggregates 1000-fold faster than WT TTR. Consistent with these observations, D18G aggregates at neutral pH (20 °C), aggregation being much faster at 37 °C. The D18G mutant is fluctuating between a natively folded state and aggregation-prone partially folded amyloidogenic intermediate structures (*21*) under physiological conditions. Unlike other disease-associated variants, D18G does not appear to be competent to form hybrid tetramers with WT subunits under physiological conditions simulated by *E. coli* coexpression or with reasonable efficiency under optimized subunit exchange conditions (4 °C). We were also unable to detect any D18G protein in the serum or the CSF of a heterozygous patient, consistent with its inability to form hybrid tetramers with WT TTR. D18G TTR can be chaperoned into a tetrameric structure utilizing small molecule ligands that bind to and stabilize the tetramer.

It is interesting that the D18G mutation, located at the end of the A-strand, is so destabilizing to the tetramer and to the tertiary structure. Identifying the neighboring residues reveals this region to harbor a number of residues known to have a strong impact on TTR tetramerization and stability (Figure 7). The following residues in the same subunit (cis) or in neighboring subunits in the tetramer (trans) are important for stability: K15 (cis) destabilizes the tetramer (*13*), V20I (cis) causes cardiac amyloidosis by destabilizing the tetramer (*18*), A25T (cis) induces CNS amyloidosis by severe tetramer and monomer destabilization (*22*), F87M (trans)/L110M (cis) at the subunit interfaces can be introduced to engineer TTR to be monomeric (*16*), L111M (cis and trans) at the subunit interface is associated with cardiac amyloidosis (*23*), Y78F (cis) that removes a hydrogen bond to D18 severely destabilizes the tetramer (*24*), Y114C (trans) is associated with CNS amyloidosis (*25*), T119M (trans) functions as a trans suppressor of amyloid formation (*10*), and V122I at the subunit interface causes cardiac amyloidosis by destabilizing the tetramer (*15*).

Mutations that destabilize the TTR tetramer predispose an individual to disease; however, thermodynamic stability alone does not reliably predict systemic amyloid disease severity. We have shown that mutations in transthyretin (TTR) also influence the kinetics of tetramer dissociation, with rapid rates exacerbating and slow rates reducing amyloidogenicity and thus disease severity (*14*). It is therefore reasonable to predict that the marked kinetic and thermodynamic destabilization associated with the D18G TTR would lead to an early onset severe systemic disease, but this is not the case. While the D18G CNS phenotype is devastating, onset occurs in the fifth decade (average 44 years) without peripheral neuropathy symptoms. The levels of D18G TTR in the plasma are undetectable, seemingly explaining why there is no systemic amyloidosis, since the source of systemic TTR in the amyloid deposits is that secreted into the plasma by the liver. The unprecedented low stability of D18G TTR enables the quality control machinery of the cell to target D18G for degradation before secretion into the blood and/or facilitates catabolism postsecretion. Some D18G appears to make it to the blood plasma, consistent with the asymptomatic deposits observed in the kidney and heart found upon autopsy; however, the quantity is below our detection limits in plasma.

Why Does D18G Form Amyloid in the CNS? It could be that the CNS is simply more sensitive toward aggregated D18G, despite the low D18G CSF concentration. Alternatively, or in addition, impaired secretion may play a role in pathology, especially if secretion is slightly more efficient in the choroid plexus than in the liver. Typically, TTR synthesized in the choroid plexus is secreted into the CSF (*26*). We hypothesize that more D18G may be able to escape the quality control machinery within the choroid plexus than in hepatocytes owing to chemical chaperoning by the high local T_4 concentration in the former tissue (*27*, *28*), only to misfold later in the CSF where the T_4 concentration is insufficient to stabilize the tetramer. While experiments within demonstrate that T_4 can in fact stabilize D18G tetramers, future cell-based experiments will be required to provide compelling evidence for such a mechanism.

Considerations for a Therapeutic Strategy. Liver transplantation (LT) is the only known treatment for FAP, wherein the variant gene is replaced by the WT gene in the organ supplying protein to the blood (*29*). However, LT will not be useful for D18G CNS disease because the amyloidogenic protein is synthesized in the choroid plexus. We may be able to utilize the tetramer-stabilizing drug candidates being developed by this laboratory to inhibit CNS amyloidosis. However, chaperoning the D18G-containing tetramers out of the choroid plexus and the liver by tetramer binding small molecule ligands could prove to be deleterious for the patient if tetramer stabilization is not sustainable postsecretion. Hence, the D18G TTR variant may be a more challenging target than other TTR variants studied to date that are secreted predominatly as tetramers (*14*, *30*). The 3,3′,5,5′-tetrachlorobiphenyl-4,4′-diol was the most effective compound at tetramerizing D18G TTR and preventing its aggregation at 37 °C. Not surprisingly, it is the highest affinity binder to WT TTR of which we are aware. Clearly, a better understanding of the basis for the low CSF D18G concentration will be required to develop an optimal small molecule therapeutic strategy for CNS amyloidosis.

ACKNOWLEDGMENT

We thank H. Purkey for helpful discussions and S. Deechongkit for initial analytical ultracentrifugation measurements.

SUPPORTING INFORMATION AVAILABLE

One figure showing deconvoluted ESI mass spectra of intact immunoprecipitated TTR from serum of a normal individual and a D18G patient and one figure depicting the soluble fraction of coexpressed D18G TTR and FT_2-WT TTR. This material is available free of charge via the Internet at http://pubs.acs.org.

REFERENCES

1. Westermark, P., Sletten, K., Johansson, B., and Cornwell, G. G. (1990) *Proc. Natl. Acad. Sci. U.S.A. 87*, 2843−2845.
2. Jacobson, D. R., Pastore, R. D., Yaghoubian, R., Kane, I., Gallo, G., Buck, F. S., and Buxbaum, J. N. (1997) *N. Engl. J. Med. 336*, 466−473.
3. Vidal, R., Garzuly, F., Budka, H., Lalowski, M., Linke, R. P., Brittig, F., Frangione, B., and Wisniewski, T. (1996) *Am. J. Pathol. 148*, 361−366.
4. Garzuly, F., Vidal, R., Wisniewski, T., Brittig, F., and Budka, H. (1996) *Neurology 47*, 1562−1567.
5. Harkany, T., Garzuly, F., Csanaky, G., Luiten, P. G., Nyakas, C., Linke, R. P., and Viragh, S. (2002) *Br. J. Dermatol. 146*, 674−679.
6. Lashuel, H. A., Wurth, C., Woo, L., and Kelly, J. W. (1999) *Biochemistry 38*, 13560−13573.
7. White, J. T., and Kelly, J. W. (2001) *Proc. Natl. Acad. Sci. U.S.A. 98*, 13019−13024.
8. Lim, A., Prokaeva, T., McComb, M. E., O'Connor, P. B., Theberge, R., Connors, L. H., Skinner, M., and Costello, C. E. (2002) *Anal. Chem. 74*, 741−751.
9. Philo, J. S. (1999) *Anal. Biochem. 279*, 151−163.
10. Hammarström, P., Schneider, F., and Kelly, J. W. (2001) *Science 293*, 2459−2461.
11. Schneider, F., Hammarström, P., and Kelly, J. W. (2001) *Protein Sci. 10*, 1606−1613.
12. Oza, V. B., Smith, C., Raman, P., Koepf, E. K., Lashuel, H. A., Petrassi, H. M., Chiang, K. P., Powers, E. T., Sachettinni, J., and Kelly, J. W. (2002) *J. Med. Chem. 45*, 321−332.
13. Hammarström, P., Jiang, X., Deechongkit, S., and Kelly, J. W. (2001) *Biochemistry 40*, 11453−11459.
14. Hammarström, P., Jiang, X., Hurshman, A. R., Powers, E. T., and Kelly, J. W. (2002) *Proc. Natl. Acad. Sci. U.S.A. 99*, 16427−16432.
15. Jiang, X., Buxbaum, J. N., and Kelly, J. W. (2001) *Proc. Natl. Acad. Sci. U.S.A. 98*, 14943−14948.
16. Jiang, X., Smith, C. S., Petrassi, H. M., Hammarström, P., White, J. T., Sacchettini, J. C., and Kelly, J. W. (2001) *Biochemistry 40*, 11442−11452.
17. Lai, Z., Colon, W., and Kelly, J. W. (1996) *Biochemistry 35*, 6470−6482.
18. Jenne, D. E., Denzel, K., Blatzinger, P., Winter, P., Obermaier, B., Linke, R. P., and Altland, K. (1996) *Proc. Natl. Acad. Sci. U.S.A. 93*, 6302−6307.
19. Tachibana, N., Tokuda, T., Yoshida, K., Taketomi, T., Nakazato, M., Li, Y. F., Masuda, Y., and Ikeda, S. (1999) *Amyloid 6*, 282−288.
20. Yamamoto, K., Hsu, S. P., Yoshida, K., Ikeda, S., Nakazato, M., Shiomi, K., Cheng, S. Y., Furihata, K., Ueno, I., and Yanagisawa, N. (1994) *Muscle Nerve 6*, 637−641.
21. Liu, K., Cho, H. S., Lashuel, H. A., Kelly, J. W., and Wemmer, D. E. (2000) *Nat. Struct. Biol. 7*, 754−757.
22. Sekijima, Y., Hammarström, P., Matsumura, M., Shimizu, Y., Iwata, M., Tokuda, T., Ikeda, S., and Kelly, J. W. (2003) *Lab. Invest. 83*, 409−418.
23. Ranlov, I., Alves, I. L., Ranlov, P. J., Husby, G., Costa, P. P., and Saraiva, M. J. (1992) *Am. J. Med. 93*, 3−8.
24. Redondo, C., Damas, A. M., Olofsson, A., Lundgren, E., and Saraiva, M. J. (2000) *J. Mol. Biol. 304*, 461−470.
25. Ikeda, S., Nakazato, M., Ando, Y., and Sobue, G. (2002) *Neurology 58*, 1001−1007.
26. Schreiber, G., Aldred, A. R., Jaworowski, A., Nilsson, C., Achen, M. G., and Segal, M. B. (1990) *Am. J. Physiol. 258*, R338−R345.
27. Dickson, P. W., Aldred, A. R., Menting, J. G., Marley, P. D., Sawyer, W. H., and Schreiber, G. (1987) *J. Biol. Chem. 262*, 13907−13915.
28. Palha, J. A., Fernandes, R., de Escobar, G. M., Episkopou, V., Gottesman, M., and Saraiva, M. J. (2000) *Endocrinology 141*, 3267−3272.
29. http://www.fapwtr.org/ (Familial Amyloidotic Polyneuropathy World Transplant Register).
30. Lashuel, H. A., Lai, Z., and Kelly, J. W. (1998) *Biochemistry 37*, 17851−17864.

BI027319B